RSC Advances

ROYAL SOCIETY OF CHEMISTRY

www.rsc.org/advances

Graphical Abstract

A BODIPY/pyrene-based chemodosimetric fluorescent chemosensor for selective sensing of hydrazine in the gas and aqueous solution state and its imaging in living cells

Ajit Kumar Mahapatra, Rajkishor Maji, Kalipada Maiti, Saikat Kumar Manna, Sanchita Mondal, Syed Samim Ali, Srimanta Manna, Prithidipa Sahoo, Sukhendu Mandal, Md Raihan Uddin and Debasish Mandal

RSC Advances
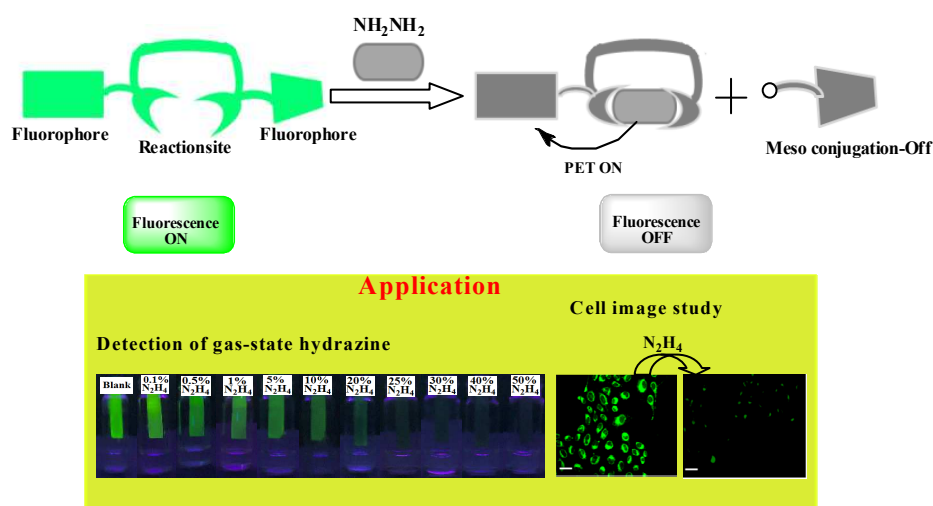
ARTICLE TYPE

A BODIPY/pyrene-based chemodosimetric fluorescent chemosensor for selective sensing of hydrazine in the gas and aqueous solution state and its imaging in living cells

Ajit Kumar Mahapatra,[*a] Rajkishor Maji,[a] Kalipada Maiti,[a] Saikat Kumar Manna,[a] Sanchita Mondal,[a]

5 **Syed Samim Ali,[a] Srimanta Manna,[a] Prithidipa Sahoo,[b] Sukhendu Mandal,[c] Md Raihan Uddin [c] and**

Debasish Mandal [d]

A BODIPY-based pyrenebutyrate-linked (**BPB**) chromogenic and fluorogenic probe was synthesized and characterized for the specific
10 detection of hydrazine. In the presence of hydrazine, BODIPY-based pyrenebutyrate was selectively deprotected, produces *switch off meso*-phenoxyBODIPY along with a color change from yellow to brown, allowing colorimetric detection of hydrazine by the naked eye. Selectivity experiments proved **BPB** has excellent selectivity to hydrazine over other environmentally abundant ions and common amine-containing species. Probe **BPB** was also successfully applied in the vapor hydrazine detection into a solid state over other interfering volatile analytes. Furthermore, the probe **BPB** coated with silica gel TLC plates could act as a visual and fluorimetric probe for hydrazine
15 vapor detection. The probe (**BPB**) has been shown to detect hydrazine up to 1.87 μM at pH 7.4. DFT and TDDFT calculations were performed in order to demonstrate the sensing mechanism and the electronic properties of probe and hydrazinolysis product. **BPB** can also be used for the detection of hydrazine in Vero cells without appreciable interference from other biologically abundant analytes.

20 ## Introduction

The development of selective fluorescent chemosensors to provide signals in response to chemically, biologically and environmentally important small molecules is an interesting area of contemporary research in supramolecular chemistry.[1] In this
25 regard, the development of a new strategy for molecular sensors involves the application of analyte triggered selective transformations of chemosensor derivatives to yield signaling on-off fluorochromes based on versatile dyes of BODIPY, rhodamine, and fluorescein.[2-4]
30 Hydrazine is an important chemical reagent such as highly reactive base and strong reducing agent used in organic group transformation. For instance, in industries, hydrazine is employed as a corrosion inhibitor for boilers due to strong reducing power to scavenge oxygen, pharmaceutical intermediate, catalyst,
35 emulsifier and antioxidant agent acts as a preservative in nuclear and electrical power plants.[5] Hydrazine also plays important roles in the preparation of pesticides, emulsifiers, drug intermediates, photography chemicals, and dyes in various chemical industries.[6] It is famous as a high-energy fuel in missiles, satellites and
40 rocket–propulsion systems due to its flammable and detonable characteristics.[7] In contrast to its usefulness, carcinogenic and toxic effects of hydrazine potentially lead to serious environmental contamination and serious health risks during its

manufacture, use, transport and disposal procedures. Hydrazine
45 vapor and its water solutions, however, are highly toxic to humans and animals causes severe damage to the liver, lungs, kidneys, central nervous system and other documented adverse systemic health effects includes irritation of eyes, nose, and throat, temporary blindness, dizziness, nausea, pulmonary edema,
50 coma, and blood abnormalities and non-specific chronic illnesses.[8] Therefore, hydrazine has been classified as a carcinogenic substance by the U.S. Environmental Protection Agency (EPA) with allowable threshold limit value (TLV) of 10 ppb,[9-10] which provides an incentive to research for new
55 analytical approaches capable of determining trace level of hydrazine are always required.
Various traditional analytical techniques for the detection of hydrazine are available, including electrochemical analysis[11] and chromatography,[12] including gas chromatography,[13] HPLC,[14]
60 coulometry,[15] potentiometry,[16] titrimetry,[17] capillary electrophoresis[18] and so on.[19] Spectrophotometry using colored derivatives, such as p-dimethylaminobenzaldehyde[20] and chlorosalicylaldehyde,[21] is also used to detect hydrazine. However, these methods are not only complex and time
65 consuming, but also impractical for in vivo hydrazine analysis because of their post-mortem processing and destruction of tissues and cell contents. Among several detection strategies,

RSC Advances Accepted Manuscript

fluorescent techniques are extremely attractive due to their high sensitivity, low cost, easy implementation, and real-time detection.[22-23] Till now, only a few fluorescent chemodosimeters for hydrazine have been reported, and almost all of them were designed based on the deprotection or chemical transformation of a protecting group by a specific deprotecting agent or analyte.[24-28] For example, the fluorescent sensing system developed by Chang *et al.*,[29] showed the selective deprotection of levulinated coumarin inpresence of hydrazine to a chemosensor to date in DMSO-water. The sensing system reported by Peng *et al.*,[30] showed a ratiometric hydrazine-selective NIR probe based on cyanine dye via deprotection of acetyl group in aqueous-organic solvent. Therefore, it still remains a challenge to develop effective hybrid fluorescent probe with suitable reactive zone can act as good chemodosimetric chemosensor for the recognition of molecular species, though such systems are limited in the literature in case of hydrazine sensing. Furthermore, fewer sensors have been applied to vapor sensing.[31-32] Some of these current probes could only be utilized in low pH (pH $<$ 5) conditions[33-34] which would limit their application in physiological condition. Thus, developing a new fluorescence method of monitoring hydrazine in living cells or sensing vapor hydrazine remains a significant challenge.

Our research group has been involved in the synthesis of various chemosensors-based BODIPY-pyrene conjugates for the selective recognition of ions and molecules.[35-36] We recently reported the selective detection of anions and CNS active alkaloids using BODIPY, pyrene and carbazole based chemosensor. Therefore, it is of prime interest to develop BODIPY-pyrene-based hybrid reactive molecular systems to provide better sensitivity and selectivity toward sensing of toxic molecules. With this in mind, in the present paper, the synthesis and characterization of BODIPY-pyrene conjugates of chemodosimeter, **BPB** and their selective recognition behavior toward hydrazine have been reported. Here two fluorophores were connected in the chemodosimeter **BPB**, because these two fluorophores has high quantum yields, high extinction coefficient, and both their excitation and emission wavelengths are in the visible region.[40] Considering that hydrazine shows strong nucleophilicity towards ester groups, the specific chemical reaction between dosimeter molecule **BPB** and hydrazine yielded the products of hydrazone and phenolate ion of BODIPY respectively. After the hydrazinolysis, the original phenolic form of the hidden probe BODIPY becomes free again, which affected the intramolecular electron density distribution of BODIPY in the meso position, therefore resulting in ICT-induced absorption and an efficient photoinduced electron transfer (PET) quenching fluorescence responses to hydrazine in solution. To the best of our knowledge, this is the first example of a chemodosimetric detection of solution as well as vapour hydrazine using BODIPY-pyrene hybrid fluorophores, which shows ON-OFF behavior due to both PET and ICT processes in the BODIPY-pyrene conjugate after hydrazinolysis. These conjugate was also demonstrated first successful intracellular application as potential live-cell fluorescence imaging agents upon treatment with hydrazine.

Experimental Section

General Information and Materials. Unless otherwise mentioned, materials were obtained from commercial suppliers and were used without further purification. ^{1}H and ^{13}C NMR spectra were recorded on a Brucker 400 MHz instrument. For NMR spectra, DMSO-d_6 was used as solvent using TMS as an internal standard. Chemical shifts are expressed in δ ppm units. Mass spectra were carried out using a Waters QTOF Micro YA 263 mass spectrometer. UV–visible and fluorescence spectra measurements were performed on a JASCO V530 and a Photon Technology International (PTI-LPS-220B) spectrofluorimeter respectively. Elemental analysis of the compounds was carried out on Perkin-Elmer 2400 series CHNS/O Analyzer. Chemicals and solvents used for the synthesis of receptor were purchased from Sigma Aldrich Chemical Co. (USA) and used without further purification. Salts of different cations, anions and amines were purchased from Spectrochem Pvt Ltd. (India). The following abbreviations are used to describe spin multiplicities in ^{1}H NMR spectra: s = singlet; d = doublet; t = triplet; m = multiplet.

General method of UV-vis and fluorescence titration. For UV-vis and fluorescence titrations, stock solution of sensor **BPB** was prepared (c = 1 x 10^{-5} ML^{-1}) in H$_2$O–DMSO (3:7, v/v) solution (10 mM HEPES buffer, pH 7.4).The solution of the guest cations, anions and amines in the order of 2 x 10^{-4} ML^{-1} was also prepared in H$_2$O–DMSO (3:7, v/v) solution (10 mM HEPES buffer, pH 7.4). The test solution of sensor **BPB** was prepared by proper dilution method. The spectra of these solutions were recorded by means of UV-vis and the fluorescence methods. All the solvents were purchased from local suppliers and were distilled by standard procedure before use.

Cell Culture. Vero cell (Vero 76, ATCC No CRL-1587) lines were prepared from continuous culture in Dulbecco's modified Eagle's medium (DMEM, Sigma Chemical Co., St. Louis, MO) supplemented with 10% fetal bovine serum (Invitrogen), penicillin (100 μg/mL), and streptomycin (100 μg/mL). The Vero 76 were obtained from the American Type Culture Collection (Rockville, MD) and maintained in DMEM containing 10% (v/v) fetal bovine serum and antibiotics in a CO$_2$ incubator. Cells were initially propagated in 75 cm^2 polystyrene, filter-capped tissue culture flask in an atmosphere of 5% CO$_2$ and 95% air at 37°C in CO$_2$ incubator. When the cells reached the logarithmic phase, the cell density was adjusted to 1.0 x 10^5 per/well in culture media. The cells were then used to inoculate in a glass bottom dish, with 1.0 mL (1.0 x 10^4 cells) of cell suspension in each dish. After cell adhesion, culture medium was removed. The cell layer was rinsed twice with phosphate buffered saline (PBS), and then treated according to the experimental need.

Cellular Imaging Methodology. For fluorescence imaging studies Vero cells, 1 x 10^4 cells in 1000 μL of medium, were seeded on sterile 35 mm Petri dish, glass bottom culture dish (ibidi GmbH, Germany), and incubated at 37 °C in a CO$_2$ incubator for 10 hours. Then cells were washed with 500 μL

DMEM followed by incubation with final concentration of 1.0 x 10^{-6} M **BPB** probe dissolved in 500 μL DMEM at 37°C for 1 h in a CO$_2$ incubator and observed under an Olympus IX71 microscope. Images analyzed by Image-pro plus (version 6.3) with excitation at nearby 495 nm FITC filter, and emit at nearby 519 nm. The cells were again washed thrice with phosphate buffered saline PBS (pH 7.4) to remove any free **BPB** probe and incubated in PBS containing NH$_2$-NH$_2$ to a final concentrations of 1.0 x 10^{-4} M, incubated for 30 min followed by washing with PBS three times to remove excess NH$_2$-NH$_2$ outside the cells and images were captured.

Synthesis of Compound (BPB). Compound (2) (100 mg, 0.294 mmol), γ-oxo-1-pyrenebutyric acid (89 mg, 0.294 mmol), EDC (56.4 mg, 0.294 mmol) and DMAP (35.9 mg, 0.294 mmol) in dichloromethane (30 mL) was stirred at room temperature for 24 h. Then water was added to the solution and extracted with CH$_2$Cl$_2$. The organic layer was washed with water and dried over MgSO$_4$. After concentration of solvent, the residue was purified *via* chromatography with silica gel (10% hexane in CHCl$_3$) to afford **BPB** as a reddish brown solid (yield 81%). M.P = 233–235 °C. ^{1}H NMR (d$_6$-DMSO, 400 MHz) δ(ppm): 8.926 (d, 1H, Ar-H, J= 9.6 Hz), 8.681 (d, 1H, Ar-H, J= 8.0 Hz), 8.415 (t, 3H, Ar-H, J= 7.8 Hz), 8.352 (d, 2H, Ar-H, J= 8.0 Hz), 8.292 (t, 1H, Ar-H, J= 7.0 Hz), 8.174 (t, 1H, Ar-H, J= 7.6 Hz), 7.431 (dd, 4H, Ar-H, J= 6.8 Hz, J= 6.4 Hz), 6.181 (s, 2H), 3.767 (t, 2H, pyrene -COCH$_2$-, J= 6.2 Hz), 3.174 (t, 2H, ester – OCOCH$_2$-, J= 6.0 Hz), 2.546 (s, 6H), 1.301 (s, 6H). ^{13}C NMR (d$_6$-DMSO, 100 MHz) δ(ppm): 14.58, 31.11, 72.46, 76.37, 88.77, 106.11, 121.95, 122.94, 123.84, 124.05, 124.67, 124.93, 125.15, 125.47, 126.34, 127.15, 127.24, 127.57, 127.64, 128.09, 129.68, 130.25, 130.67, 130.86, 132.02, 134.67, 139.35, 144.95, 162.75, 184.51, 206.71. TOF MS ES+, m/z = 647.0407 [**BPB**+Na]$^+$; calculated, 647.4727 Anal. Cald for C$_{39}$H$_{31}$N$_2$O$_3$BF$_2$; C, 75; H, 5 ; N, 4.486 Found: C, 75.12; H, 4.92; N, 4.46%.

Results and discussion

The chemodosimeter **BPB** was synthesized by going through the steps given in Scheme 1. Initially, BODIPY part was synthesized by the condensation of 4-hydroxybenzaldehyde with 2,4-dimethylpyrrole according to a published procedure.[36] The final dosimeter molecule, **BPB** has been synthesized in a single step by reacting BODIPY with γ-oxo-1-pyrenebutyric acid in presence of coupling agent EDC/DMAP in dichloromethane at room temperature. All the synthesized molecules were well characterized by various analytical and spectral techniques. To understand the reactive properties of **BPB** towards hydrazine, studies were carried out by emission, absorption, and ^{1}H NMR spectroscopy, and the species of recognition has been addressed by mass spectrometry and computations based on the density functional theory (DFT). The detection of hydrazine vapor by silica gel plate is also demonstrated. The pyridomethene–BF$_2$ complex dye is selected as a fluorescent transducer due to its high fluorescence intensity both in solution and in solid state.
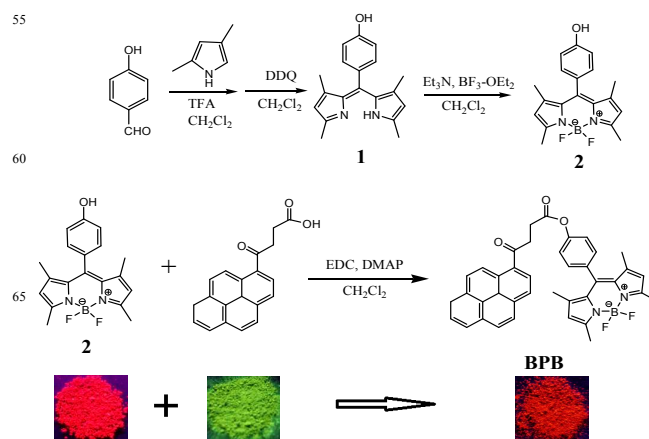
Scheme 1. Schematic representation of synthesis of **BPB**. Solid-state fluorescence images of 2, γ-oxo-1-pyrenebutyric acid and **BPB** under 366 nm ambient light irradiation.

In order to find the suitability of **BPB** to react hydrazine in aqueous buffer solution at physiological pH, fluorescence titrations were carried out in different solvent mixture at room temperature. As we know, nucleophilic substitution reactions are better conducted in organic solutions. Therefore, we firstly investigated the emission properties of probe **BPB** in pure DMSO. We found that the addition of 2 equiv. of hydrazine could result in an immediate drop of fluorescence intensity at both 456 and 516 nm respectively. As shown in Figure S7 in the Supporting Information, the fluorescence spectra changes in different aqueous HEPES buffer in H$_2$O–DMSO solution are similar to those in pure DMSO but the drop of fluorescence intensity is slower than that in pure DMSO. We speculate this phenomenon was probably due to the hydrogen bond between hydrazine and water in aqueous solution that weakened the nucleophilicity of hydrazine to **BPB** and then decreased the reaction speed. Finally, the fluorescence signalling behaviour of BODIPY-pyrene-based probe **BPB** was investigated in an optimized aqueous solution HEPES buffer (pH 7.4, 10 mM) in H$_2$O–DMSO (3:7, v/v) at room temperature.
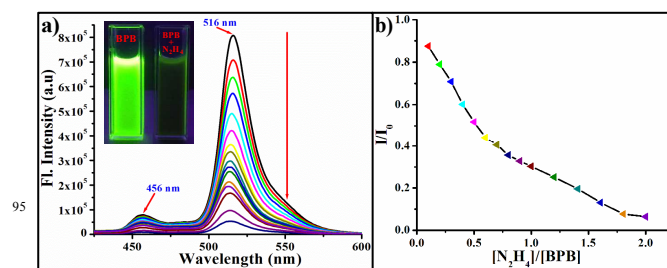
Figure 1. (a) Fluorescence spectra (excitation at 356 nm) of sensor **BPB** (c = 1 x 10^{-5} ML^{-1}) in H$_2$O–DMSO (3:7, v/v) solution (10 mM HEPES buffer, pH 7.4) in the presence of 0 − 2.0 equiv. of hydrazine and (b) the relative fluorescence intensity (I/I$_0$) as a function of [N$_2$H$_4$]/[**BPB**] mole ratio.

The probe **BPB** exhibit very strong emission bands at 456 and 516 nm due to pyrene and BODIPY moieties respectively when

excited at 356 nm in 3:7 H₂O–DMSO mixture at pH 7.4 to have an effective HEPES buffer concentration of 10 mM. By contrast, upon gradual addition of hydrazine to the probe **BPB**, the emission intensity bands at 456 and 516 nm sharply decreases
5 along with the solution color change from bright green to colorless under a UV lamp. When the concentration of hydrazine reached 2 equiv., a maximal fluorescence decrease (up to a 15.5-fold decrease at 516 nm) was observed (Figure 1). A plot of fluorescence intensity as a function of added [Hydrazine]/[**BPB**]
10 mole ratio (Figure 1b) shows a stoichiometry of 1:1 between the probe and hydrazine and the intensity goes to lowest value at ≥1 equiv.

The observed fluorescence off may be viewed as follows. We speculate that the signalling change was due to the selective
15 deprotection of the 4-oxo-4-pyrenylbutyrate of probe **BPB** by hydrazine and generate hidden phenolate unit of BODIPY(3). The product generated by the reaction of probe **BPB** with hydrazine is confirmed to be compound 3 and 4 (Scheme 2) by mass spectrometry analysis (Figure S8 in the Supporting
20 Information). Our previous work[36-39] has demonstrated that a phenoxy substituent or any electron donating group at the *meso* (8) position of the BODIPY core plays crucial role for photoinduced-electron-transfer (PET)-based quenching of the emission. To confirm the validity of the proposed sensing
25 mechanism, a solution of probe **BPB** was analyzed by ^{1}H NMR in the absence and presence of hydrazine. The protons of BODIPY moieties moved up field when hydrazine was added, which obviously suggested that the probe **BPB** totally converted to oxonium with the removal of the 4-oxo-4-pyrylbutyrate
30 (Scheme 2). Thus, the detection limit of the probe for hydrazine was calculated (2σ/slope) to be 1.87 μM (Figure S9 in the Supporting Information).

To prove the selectivity of probe **BPB**, the competitive fluorescence titrations were carried out in the presence of
35 common anions and cations, redox molecules and amines. As shown in Figure 2, upon addition of 30 equiv. of guest molecules or ions (the common ions included F^-, Cl^-, Br^-, I^-, CN^-, N_3^-, PO_4^{3-}, NO_3^-, S^{2-}, SO_4^{2-}, HSO_4^- (as their sodium salts), and amines (NH₂OH, ethylene diamine and NH₃) exhibited almost no
40 changes in emission behaviour.
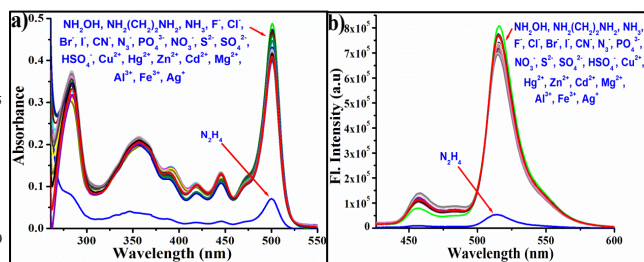
Meanwhile, the commonly encountered cations [Cu^{2+}, Hg^{2+}, Zn^{2+},
60 Cd^{2+}, Mg^{2+}, Al^{3+}, Fe^{3+} and Ag^+ (as their chloride salts)] did not cause any change to the fluorescence of probe **BPB** (Figure 2). The results indicate that the probe **BPB** has high selectivity for hydrazine over other species. This may be attributed to the unique chemical reaction between 4-oxo-4-pyrylbutyrate and hydrazine.

65
Fluorescence spectra were also recorded for the titration of probe **BPB** against hydrazine in the presence of 30 equiv of common anions and cations, redox anions and amines. None of these analyte significantly affects the emission intensity of **BPB** upon
70 the addition of hydrazine, and the titration profile is similar to that obtained for simple hydrazine titration (Figure S10 in the Supporting Information). Therefore, it can be concluded that probe **BPB** selectively reacts hydrazine even in the presence of other analytes.
75 In order to ascertain the reactivity of hydrazine by probe **BPB**, absorption titrations were carried out by adding varying concentrations of hydrazine to a fixed concentration (c = 1 x 10^{-5} M) of **BPB**. We found that the addition of trace amounts of hydrazine causes the absorption and fluorescence
80 signal to change rapidly, which is very important for real-time detection. Therefore, the following titration experiments were carried out after gradual addition of hydrazine.

The absorption spectra of free **BPB** in aqueous DMSO (3:7 v/v) HEPES buffer (pH 7.4) exhibited different bands from 250 to 550 nm. The absorbance of 284, 356, 438 and 501 nm bands is found
85 to decrease gradually upon addition of hydrazine (Figure 3a), indicating the interaction of hydrazine with the reactive groups such as ester and carbonyl present in the probe **BPB**.

Figure 2. (a) UV-vis spectra and (b) Fluorescence spectra of **BPB** (c = 1 x 10^{-5} M) in H₂O-DMSO (3:7, v/v) solution (10 mM
55 HEPES buffer, pH 7.4) in the presence of hydrazine (2 equivalents) and other representative cations, anions and organic bases (30 equivalents each).
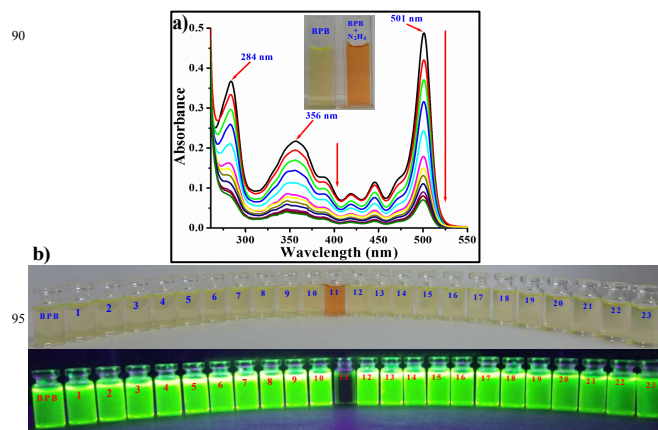
Figure 3. (a) Changes in the UV/vis absorption spectra of sensor **BPB** (c = 1 x 10^{-5} M) in H₂O–DMSO (3:7, v/v) solution (10 mM
100 HEPES buffer, pH 7.4) in the presence of 0 – 2.0 equiv. of hydrazine and (b) the photograph of visible color (top) under ambient light and visual fluorescence color (bottom) changes of sensor **BPB** with various relevant analytes in H₂O–DMSO (3:7, v/v) solution under a hand–held UV lamp (366 nm): **BPB** only;
105 (1) NH₂OH; (2) NH₂(CH₂)₂NH₂ ; (3) NH₃; (4) F^-; (5) Cl^-; (6) Br^-; (7) I^-; (8) CN^-; (9) N_3^-; (10) PO_4^{3-}; (11) N_2H_4; (12) NO_3^-; (13) S^{2-}; (14) SO_4^{2-}; (15) HSO_4^-; (16) Cu^{2+}; (17) Hg^{2+}; (18) Zn^{2+}; (19) Cd^{2+}; (20) Mg^{2+}; (21) Al^{3+}; (22) Fe^{3+} and (23) Ag^+.

The absorption behavior changed the color of the solution from light green to orange, allowing colorimetric detection of hydrazine by the naked eye. The color of the fluorescence also changed clearly from green to colorless. However the absorption titration carried out with all the other common cations and anions as well as redox anions showed no significant change, indicating their noninteractive nature with **BPB**. Even the different amines do not react to **BPB** at room temperature.

We speculate that the 4-oxo-4-pyrenylbutyrate moiety was selected as the reaction site on the fluorophore, based on a specific reactivity between **BPB** and hydrazine for the production of pyrene and BODIPY deivatives. Hydrazine was detected by hydrazinolysis of the oxo-pyrene-butarate moiety of **BPB** (Scheme 2).
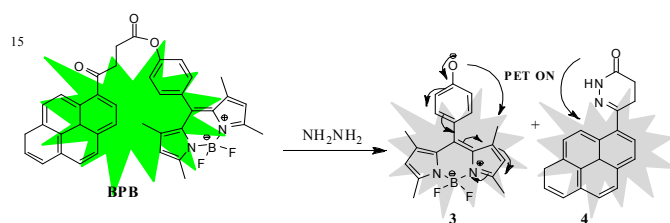
Scheme 2. Hydrazine-Selective Signaling Mechanism by **BPB**.

This reaction generated *meso*-phenoxyBODIPY(**3**) which exhibited its characteristic chromogenic and fluorescent behaviors.
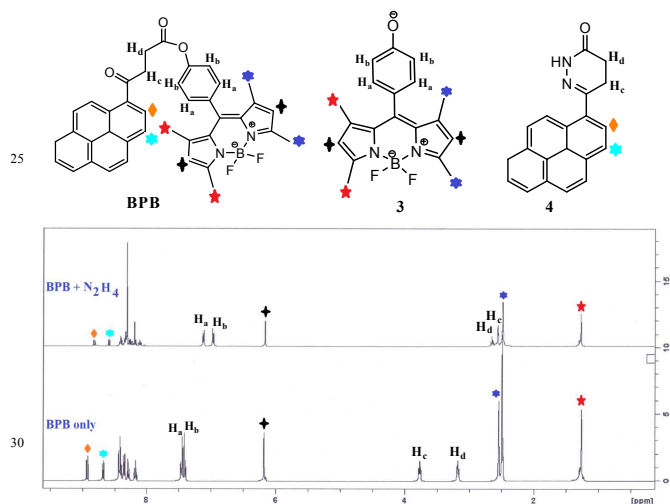
Figure 4. Partial ^{1}H NMR (400 MHz) spectra of **BPB** only and [**BPB** + N_2H_4]. [**BPB**] = 4 x 10^{-3} M, [Hydrazine] = 1 x 10^{-2} M in D_2O/DMSO-d_6 (3:7, v/v).

The reaction of **BPB** with N_2H_4 was illustrated by involving two steps, at first the nucleophilic addition-elimination to the carbonyl group at the 4-position of the 4-oxobutyrate group and then the second nucleophilic addition-elimination to the ester carbonyl with subsequent amide ring formation leading to cleavage of the ester function to release the *meso*-phenoxyBODIPY moiety. This is consistent with the hydrazine-promoted deprotection of the levulinate group.[29] We suggest that the nonfluorescent of the hydrazinolysis product, which resulted from the efficient PET

quenching of the excited state of the BODIPY moiety, but the ICT process we mentioned above is the only reason that gives rise to large changes in the absorption and emission spectra.

To confirm the validity of the proposed sensing mechanism, a solution of probe **BPB** was analyzed by ^{1}H NMR in the absence and presence of hydrazine. By ^{1}H NMR spectroscopy, resonances for the phenyl parts of BODIPY moiety of probe **BPB** were observed at 7.46 and 7.41 ppm. After hydrazine was added, the aromatic protons H_a and H_b in probe **BPB** moved up field to 7.12 and 6.93 ppm respectively, which obviously suggested that the probe **BPB** totally converted to oxonium with the removal of the oxobutyrate group and matched the characteristic chemical shift for the aromatic protons H_a and H_b in *meso*-phenoxyBODIPY. In addition, the resonances of the reaction product pyrene derivative of tetrahydropyridazinone were also observed (Figure 4). The characteristic methylene protons of H_c (pyrene -COCH$_2$-) and H_d (ester –OCOCH$_2$-) at 3.76 and 3.17 ppm respectively in probe **BPB** disappeared in probe [**BPB** +N_2H_4], and the methylene protons of H_c (pyrene -COCH$_2$-) and H_d (ester –OCOCH$_2$-) at 2.57 and 2.71 ppm respectively in pyrene derivative of tetrahydropyridazinone were clearly found, indicating the clean cleavage of the ester bond. The UV-vis and fluorescence spectrum of probe **BPB** in the presence of hydrazine was also almost identical to that of the proposed deprotection product of phenoxy BODIPY itself (Figure S11 in the Supporting Information). To further understand the mechanism of probe **BPB** with hydrazine, ESI-MS was used to test the solutions containing **BPB** and 5 equiv. hydrazine, and the peak at 341.00 instead of 647.0407 proved that the ester group had been removed and generation of new peak at 299.2 corresponds to pyrene derivative of tetrahydropyridazinone.
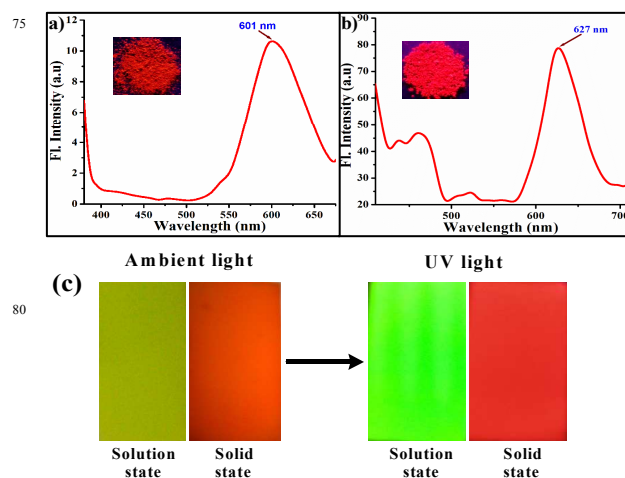
Figure 5. Fluorescence spectra of (a) **BPB** and (b) compound-2 in the solid state (film). The excitation wavelength was 356 nm and 370 nm for **BPB** and compound-2 respectively. The inset shows the solid-state fluorescence images of **BPB** and 2 under 366 nm UV-light irradiation. (c) Photographs showing the colors of **BPB** in solution and solid state on TLC plate strips under ambient (left) and UV light (right).

To understand the spectroscopic properties of the new **BPB** probe in the solid state, the solid-state absorption and emission spectra, the thin films were prepared by evaporation of 500 μM dyes in CH$_2$Cl$_2$ onto a silica plates.

5 The visual color of **BPB** is bright red in solid state, and its fluorescence spectrum is shown in Figure 5a. After dipping into a CH$_2$Cl$_2$ solution of **BPB** followed by drying, the silica gel plate looks orange, yet emits a red color under UV light (366 nm) (Figure 5c). Solid state sensors are convenient to use and much
10 easier to carry around for practical usage. As anticipated, the new dyes in the solid state display a red-shift (Δδ = 85 nm) in the emission profiles relative to in dichloromethane. In great contrast to most BODIPY dyes, which barely exhibit fluorescence in their solid-state due to the small stokes-shifts.[41-42] By sharp contrast,
15 our new **BPB** dyes have large stokes shifts, which bodes well for the solid-state emission. Indeed, **BPB** display intense reddish-orange emission in the solid state (Figure 5a).

By contrast, compound-2 shows solid-state crimson red emission (Figure 5b). Aprahamian and co-workers showed [43] that the solid-
20 state fluorescent of boron difluoride (BF$_2$) complexes depends on several parameters: (1) the planarity of the molecule, (2) the dipole moment, (3) the number of π–π interactions between neighboring dyes, and (4) the peripheral decoration of BODIPY by bulky substituents (preferably in meso position) in order to
25 avoid significant aggregation caused quenching (ACQ).[44-45] So this luminescent compound show interesting optical properties both in solution and the solid-state.[46-48]

The fluorescence spectra of **BPB** in different solvents were measured as shown in Figure 6b. The emission displays a
30 significant solvatochromic shift to longer wavelength upon decreasing the solvent polarity. The polarity of the system from acetonitrile to toluene/hexane led to a slight to moderate red shift of the absorption/emission maxima.
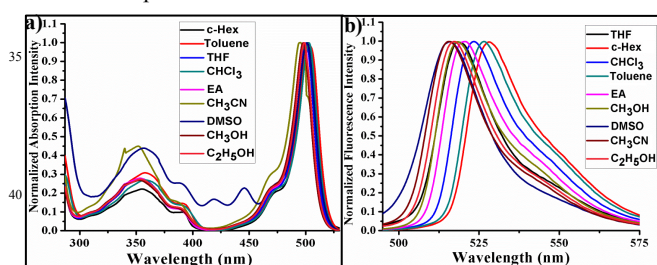
Figure 6. Normalized (a) Absorption and (b) emission spectra of **BPB** recorded in different solvents [λ$_{exc}$= 356 nm].

45 The shift of λ$_{em}$ increases from 516 nm in acetonitrile up to 528 nm in a hexane nonpolar solvent. It indicates that the dipole moment of **BPB** after the photo-excitation was not so much increased as there is no ICT present in the molecule.

To get insight into the optical response of probe **BPB** to
50 hydrazine, the probe **BPB** and the corresponding products obtained from the reaction between probe **BPB** and hydrazine were examined by density function theory (DFT) and time-dependent density function theory (TDDFT) calculations at the

TDB3LYP/6-311G(*d,p*)//B3LYP/6-31G(d,p)　　level　　of　　the
55 Guassian 09 program.[49]
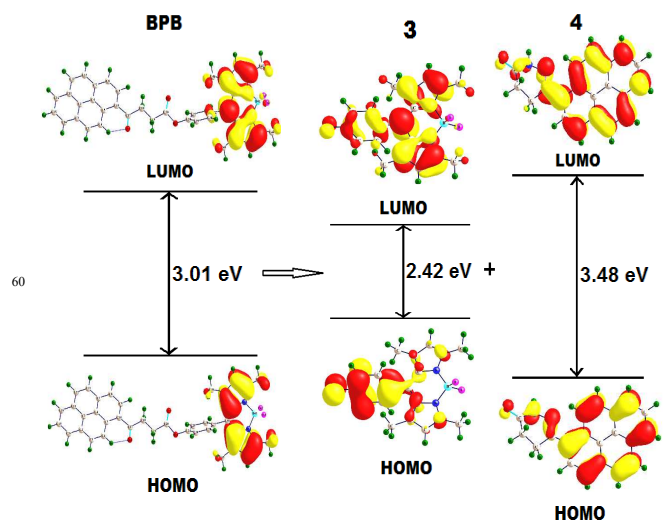
65 **Figure 7.** Calculated (B3LYP/6-311G(d,p)//B3LYP/6-31G(d,p) level) geometry and HOMO−LUMO energy levels and the interfacial plots of the orbitals for sensor **BPB**, **3** and **4** in solvent phase.

The optimized geometries and calculated electron distributions in
70 the frontier molecular orbitals HOMO and LUMO of **BPB** and the two fragmented products of BODIPY moiety and pyrene-hydrazone moiety are shown in Figure 7. In particular, for the probe **BPB**, both the HOMO and LUMO are mostly localized at the BODIPY moiety. As well as planar BODIPY ring fragment is
75 almost perpendicular to the adjacent phenyl part with dihedral angle 89.5^0. The major chromophore BODIPY adopts a nonplanar conformation with other part of the probe, and hence the ICT character of the sensor is only very weak as result no absorption and emission shift happen. Only the formation of the
80 local emission (LE) bands at 501 and 453 nm for BODIPY and pyrene moieties were observed. The formation of the LE emission bands at 501 and 453 nm in the hydrazine products are likely due to the nonplanar and nonconjugated character of the meso position.

85 In addition, we also performed time-dependent density function theory (TD-DFT) calculations for the reactant as well as both the product also. The vertical transitions *i.e,* the calculated λmax, main orbital transition, and oscillator strength (*f*) are listed in Table S1 in the Supporting Information. In the case of the **BPB**
90 probe, TDDFT calculations provided absorption band at ~427, ~393 and ~255 nm belonging to the S$_0$→S$_1$ (*f* = 0.5740), S$_0$→S$_4$ (*f* = 0.5401)and S$_0$→S$_{28}$(*f* = 0.4601) energy states respectively (Table S1 and Table S2 in the Supporting Information). The main contributing transitions are S$_0$→S$_1$ (~ 98.0%) and S$_0$→S$_4$
95 (~94.6%), which corresponds to energy states arises from HOMO→LUMO and HOMO-1→LUMO+1 respectively. These values are consistent with the absorbance bands at 438 and 356 nm obtained experimentally. In particular for BODIPY product, the MO's are majorly localized on phenoxide conjugated

BODIPY unit, and the main contribution transition comes from HOMO→LUMO (100%) with a greater oscillator strength (f = 0.3563) provided a calculated absorption band at ~577 nm, which also mainly corresponds to the absorbance band at 501 nm obtained experimentally. Similarly, the calculated band at ~386 nm of pyrene-hydrazone is assigned to the vertical major transition of HOMO → LUMO (95.6%) (Figure 7) that results from a $\pi \rightarrow \pi^*$ transition within the pyrene fragment, which mainly corresponds to the experimentally observed absorbance band at 356 nm. Notably, there is no ICT between the BODIPY and pyrene moieties, which could be the main reason for the Local Emissions (LE) of the two fluorophores.

In order to show the practical utility of **BPB** for the detection of hydrazine, we further tested whether probe **BPB** could be applicable in the detection of gas-state hydrazine that is universal during industrial processes among other vaporizable organic compounds. To make the detection experiments easy to perform and practical, test strips were used. Prior to detection, test strips were prepared by sinking the filter paper with probe **BPB** (5.0 mM) of CH_2Cl_2 solution and then dried. The probe-loaded test strips were covered on the top of jars that contained different hydrazine solution concentrations (blank, 0.1%, 0.5%, 1%, 5%, 10%, 20%, 25%, 30%, 40% and 50% in water) for 10 min at room temperature before it was ready to observe. The fluorescence color of the strips gradually faded, which proved that the fluorescence intensity of the probe on the test strips were highly dependent on the concentration of hydrazine in aqueous solution and easy to distinguish with the naked eye (Figure 8).
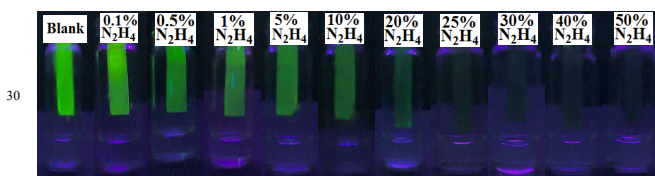
Figure 8. Fluorescence color changes of probe **BPB** (5.0 mM) coated filter paper after exposure to different concentrations of hydrazine aqueous solution. The Fluorescence color changes were collected using a hand–held UV lamp (366 nm).

Thus, one highlight of this probe is that **BPB** could identify hydrazine vapor even with a concentration as low as 0.5%, which is considerably more sensitive than the recently developed hydrazine probes.[31-32] It is noteworthy that the probe has high potential applications in hydrazine detection. Hydrazine in gaseous form often threatens human life, so our designed probe has more application potential.

We also explored opportunities for probe **BPB** to analyze hydrazine in aqueous solution for practical applications. Because hydrazine has carcinogenic properties, and has been widely used in a variety of industrial processes, hydrazine detection in aqueous samples is of interest.

Prior to living cell imaging, probe **BPB** was used to detect hydrazine in tap water and distilled water. An aliquot of hydrazine was added to water and the recoveries obtained by

BPB signals were compared in tap water and distilled water (Figure 9). The analysis of hydrazine in both solutions agreed well at hydrazine concentrations up to 2.0 x 10^{-4} M. The results show that probe **BPB** can detect hydrazine in real water samples quantitatively.
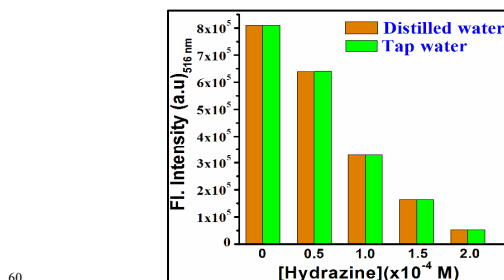
Figure 9. Fluorescence detection of hydrazine in distilled water and tap water by **BPB**. [**BPB**] = 1.0×10^{-5} M, [Hydrazine] = from 0 to 2.0×10^{-4} M in H_2O–DMSO (3:7, v/v) solution (10 mM HEPES buffer, pH 7.4) [λ_{exc} = 356 nm].

The favorable features of the probe **BPB** absorption and emission in the visible region, a significant fluorescence turn-off signal, high sensitivity, high selectivity and functioning well at physiological pH due to the interacting properties of probe **BPB** with hydrazine.
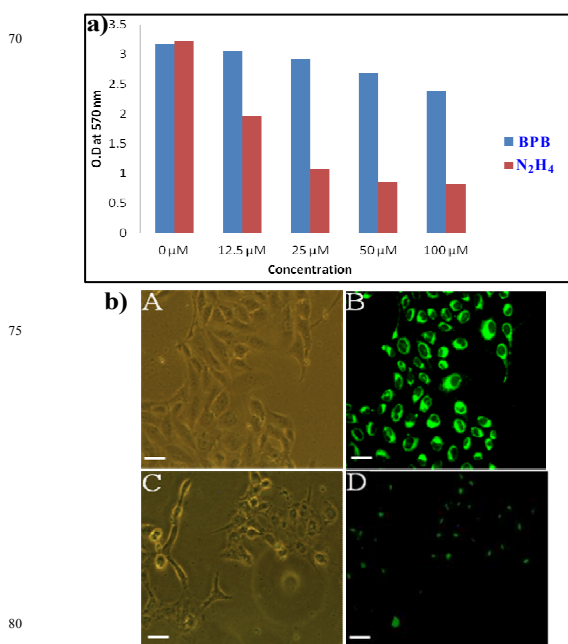
Figure 10. (a) MTT assay to determine the cytotoxic effect of Probe **BPB** and **BPB** -N_2H_4 on Vero 76 cells. (b) Fluorescence microscopic images in Vero 76 cells: (A) bright field image of the cells, pretreated with probe **BPB**, (B) only probe **BPB** at 1.0 x 10^{-6} M concentration, (C) bright field image of the cells treated with N_2H_4 at concentration 1.0 x 10^{-4} M, (D) cells treated with probe at concentration 1.0 x 10^{-6} M, N_2H_4 at 1.0 x 10^{-4} M, and switch-off fluorescence signal is detected. All images were acquired with a 40x objective lens. Scale bar represents 20 μm.

These desirable characters prompted us to evaluate the ability of the probe to image hydrazine in living cells. Prior to investigating the suitability of the probe **BPB** for imaging hydrazine in living cells, it is necessary to evaluate its cytotoxicity.

5 The standard MTT assays suggest that the probe **BPB** has low cytotoxicity to the living cells (Figure 10a). Now the stage was set for cell imaging of hydrazine. The living cells were treated with the probe **BPB** in the absence or presence of hydrazine. Vero cells incubated with **BPB** (10 μM) for 20 min at 37 ^{0}C in
10 PBS buffer with 0.5% DMSO showed strong intracellular fluorescence as shown in Figure 10b(B). By contrast, cells pre-loaded with the probe **BPB** and further incubated with hydrazine for further 10 min displayed switch-off fluorescence (Figure 10b) inside Vero cells, as observed earlier in solution studies. The
15 fluorescence microscopic analysis strongly suggested that hydrazine could readily cross the membrane barrier of the Vero cells, and rapidly sense intracellular probe **BPB** by altering the intrinsic fluorescence of **BPB**, after hydrazinolysis. It is significant to mention here that bright field images of treated cells
20 did not reveal any gross morphological changes, which suggested that Vero cells were viable. These findings open up the avenue for future in vivo biomedical applications of the sensor. Thus, **BPB** can be a suitable fluorescence chemosensing probe for hydrazine detection in biological systems.

25 ## Conclusion

A new chemosignaling probe system based on the BODIPY-pyrenebutyrate-linked (**BPB**) has been synthesized and characterized. The probe could selectively react with hydrazine through deprotection of pyrenebutyrate, resulting in an ON–OFF
30 fluorescence signal change at 516 and 456 nm respectively in a 30% aqueous DMSO solution. The selectivity and sensitivity was demonstrated on the basis of fluorescence, absorption, and ^{1}H NMR spectroscopy, ESI mass spectrometry, and visual fluorescent color changes. The significant changes in
35 fluorescence color can be observed by the naked eye as well as in the solid state. It is noteworthy that probe could identify hydrazine vapor even with a concentration as low as 0.5% within a few minutes at 25 ^{0}C when silica gel plate soaked with **BPB.** The limit of detection is 1.87 μM. The structural, electronic, and
40 emission properties of the **BPB** and its reaction products, have been demonstrated using DFT computational calculations. The TDDFT calculations reveal that the switch off fluorescence behavior of **3** is mainly due to the conjugation of electron donating group at the *meso* (8) position of the BODIPY core.
45 Additionally, probe **BPB** could be used to visualize hydrazine in living cells. This sensor has high potential as a useful tool for investigating the roles of hydrazine in biological and pathological processes.

Acknowledgment

Notes and references

^{a}Department of Chemistry, Indian Institute of Engineering Science and
55 Technology, Shibpur, Howrah-711103, West Bengal, India, Email: akmahapatra@rediffmail.com, Fax: +913326684564

^{b} Department of Chemistry, Visva-Bharati (A Central University), Santiniketan 731235, India.

^{c} Department of Microbiology,University of Calcutta, Kolkata-700019,
60 India.

^{d}Institute of Chemistry, The Hebrew University of Jerusalem, 91904 Jerusalem, Israel.

† Electronic Supplementary Information (ESI) available: [details of any supplementary information available should be included here]. See
65 DOI: 10.1039/b000000x/

1 X. Su and I. Aprahamian, *Chem. Soc. Rev.,* 2014, **43**, 1963– 1981.
2 M. E. Jun, B. Roy and K. H. Ahn, *Chem. Commun.,* 2011, **47**, 7583–7601.
70 3 J. Du, M. Hu, J. Fan, X. Peng, *Chem. Soc. Rev.,* 2012, **41**, 4511– 4535.
4 Y. Yang, Q. Zhao, W. Feng and F. Li, *Chem. Rev.,* 2013, **113**, 192–270.
5 S. D. Zelnick, D. R. Mattie, P. C. Stepaniak, *Aviat. Space Environ. Med.,* 2003, **74**, 1285– 1291.
75 6 A. Umar, M. M. Rahman, S. H. Kim and Y. B. Hahn, *Chemical Commun.,* 2008, 166– 168
7 H. W. Schiessl, *Kirk-Othmer Encyclopedia of Chemical Technology, John Wiley& Sons, Incorporation,* NJ USA, 2000, 562–607.
8 American Conference of Governmental Industrial Hygienists,
80 Documentation of Threshold Limit Values and Biological Exposure Indices, ACGIH, Cincinnati,OH, 1999.
9 G. Choudhary and H. Hansen, *Chemosphere* 1998, **37**, 801–843.
10 U.S. Environmental Protection Agency (EPA), Integrated Risk Information System (IRIS) on Hydrazine/Hydrazine Sulfate, National
85 Center for Environmental Assessment, Office of Research and Development, Washington*,* DC 1999.
11 C. Batchelor-McAuley, C. E. Banks, A. O. Simm, T. G. J. Jones and R. G. Compton, *Analyst* 2006, **131**, 106– 110.
12 D. P. Elder, D. Snodin and A. Teasdale, *J. Pharm. Biomed. Anal.,*
90 2011, **54**, 900– 910.
13 M. Sun, L. Bai and D. Q. Lui, *J. Pharm. Biomed. Anal.,* 2009, **49**, 529– 533.
14 H. Bhutani, S. Singh, S. Vir, K. K. Bhutani, R. Kumar, A. K. Chakraborti and K. C. Jindal, *J. Pharm. Biomed. Anal.,* 2007, **43**, 1213–
95 1220.
15 E. C. Olson, *Anal. Chem.,* 1960, **32**, 1545–1547.
16 J. R. Stetter, K. F. Blurton, A. M. Valentine and K. A. Tellefsen, *J. Electrochem. Soc.,* 1978, **125**, 1804–1807.
17 H. E. Malone, *Anal. Chem.,* 1961, **33**, 575–577.
100 18 J. Liu, W. Zhou, T. You, F. Li, E. Wang and S. Dong, *Anal. Chem.,* 1996, **68**, 3350-3353.
19 J. Wang and Z. Lu, *Electroanalysis* 1989, **1**, 517–521.
20 M. George, K. S. Nagaraja and N. Balasubramanian, *Talanta* 2008, **75**, 27– 31.
105 21 X. Chen, Y. Xiang, Z. Li and A. Tong, *Anal. Chim. Acta* 2008, **625**, 41– 46.
22 D. T. Quang and J. S. Kim, *Chem. Rev.,* 2010, **110**, 6280–6303.
23 A. P. Demchenko, Springer: New York 2008.
24 G. E. Collins and S. L. Rose-Pehrsson, *Analyst* 1994, **119**, 1907–
110 1913.
25 Y. D. Lin and T. J. Chow, *RSC Adv.,* 2013, **3**, 17924– 17929.

26 M. H. Lee, B. Yoon, J. S. Kim and J. L. Sessler, *Chem. Sci.,* 2013, **4**, 4121– 4126.

27 S. Goswami, S. Das, K. Aich, B. Pakhira, S. Panja, S. K. Mukherjee and S. Sarkar, *Org. Lett.,* 2013, **15**, 5412– 5415.

28 M. D. Sun, J. Guo, Q. B. Yang, N. Xiao and Y. X. Li, *J. Mater. Chem. B.,* 2014, **2**, 1846–1851.

29 M. G. Choi, J. Hwang, J. O. Moon, J. Sung and S.-K. Chang, *Org. Lett.,* 2011, **13**, 5260–5263.

30 C. Hu, W. Sun, J. F. Cao, P. Gao, J. Y. Wang, J. L. Fan, F. L. Song, S. G. Sun and X. J. Peng, *Org. Lett.,* 2013, **15**, 4022–4025.

31 L. Cui, Z. Peng, C. Ji, J. Huang, D. Huang, J. Ma, S. Zhang, X. Qian and Y. Xu, *Chem. Comm.,* 2014, **50**, 1485–1487.

32 L. Xiao, J. Tu, S. Sun, Z. Pei, Y. Pei, Y. Pang and Y. Xu, *RSC Advances.,* 2014, **4**, 41807– 41811.

33 J. Fan, W. Sun, M. Hu, J. Cao, G. Cheng, H. Dong, K. Song, Y. Liu, S. Sun and X. Peng, *Chem. Commun.,* 2012, **48**, 8117–8119.

34 M. G. Choi, J. O. Moon, J. Bae, J. W. Lee and S. K. Chang, *Org. Biomol. Chem.,* 2013, **11**, 2961-2965.

35 A. K. Mahapatra, S. Mondal, K. Maiti, S. K. Manna, R. Maji, S. Mandal, S. Goswami, D. Mondal, C. K. Quah and H.-K. Fun, *RSC Advances* 2014, **4**, 56605–56614.

36 A. K. Mahapatra, R. Maji, K. Maiti, S. S. Adhikary, C. D. Mukhopadhyay and D. Mandal, *Analyst* 2014, *139*, 309-315.

37 Q. Li, Y. Guo and S. Shao, *Analyst* 2012, **137**, 4497-4501.

38 G. Meng, S. Velayudham, A. Smith, R. Luck and H. Liu, *Macromolecules* 2009, **42**, 1995-2001.

39 J. O. Huh, Y. Do and M. H. Lee, *Organometallics* 2008, **27**, 1022–1025.

40 N. Boens, V. Leen and W. Dehaen, *Chem. Soc. Rev.,* 2012, **41**, 1130–1172.

41 J. Araneda, E. Piers, B. Heyne, M. Parvez and R. McDonald, *Angew. Chem., Int. Ed.,* 2011, **50**, 12214–12217.

42 D. Zhao, G. Li, D. Wu, X. Qin, P. Neuhaus, Y. Cheng, C. Yang, Z. Lu, X. Pu, C. Long and J. You, *Angew. Chem., Int. Ed.,* 2013, **52**, 13676–13680.

43 Y. Yang, X. Su, C. N. Carrol and I. Aprahamian, *Chem. Sci.,* 2012, **3**, 610–613.

44 H. Lu, Q. Wang, L. Gai, Z. Li, Y. Deng, X. Xiao, G. Lai and Z. Shen, *Chem. Eur. J.,* 2012, **18**, 7852–7861.

45 L. Gai, H. Lu, B. Zou, G. Lai, Z. Shen and Z. Li, *RSC Adv.,* 2012, **2**, 8840–8846.

46 J. Massue, D. Frath, G. Ulrich, P. Retailleau and R. Ziessel, *Org. Lett.,* 2012, **14**, 230-233.

47 J. Massue, P. Retailleau, G. Ulrich and R. Ziessel, *New. J. Chem.,* 2013, **37**, 1224–1230.

48 J. Massue, D. Frath, P. Retailleau, G. Ulrich and R. Ziessel, *Chem. Eur. J.,* 2013, **19**, 5375–5386.

49 Gaussian 09, Revision D.01, M. J. Frisch, G. W. Trucks, H. B. Schlegel, G. E. Scuseria, M. A. Robb, J. R. Cheeseman, G. Scalmani, V. Barone, B. Mennucci, G. A. Petersson, H. Nakatsuji, M. Caricato, X. Li, H. P. Hratchian, A. F. Izmaylov, J. Bloino, G. Zheng, J. L. Sonnenberg, M. Hada, M. Ehara, K. Toyota, R. Fukuda, J. Hasegawa, M. Ishida, T. Nakajima, Y. Honda, O. Kitao, H. Nakai, T. Vreven, J. A. Montgomery, Jr., J. E. Peralta, F. Ogliaro, M. Bearpark, J. J. Heyd, E. Brothers, K. N. Kudin, V. N. Staroverov, R. Kobayashi, J. Normand, K. Raghavachari, A. Rendell, J. C. Burant, S. S. Iyengar, J. Tomasi, M. Cossi, N. Rega, J. M. Millam, M. Klene, J. E. Knox, J. B. Cross, V. Bakken, C. Adamo, J. Jaramillo, R. Gomperts, R. E. Stratmann, O. Yazyev, A. J. Austin, R. Cammi, C. Pomelli, J. W. Ochterski, R. L. Martin, K. Morokuma, V. G. Zakrzewski, G. A. Voth, P. Salvador, J. J. Dannenberg, S. Dapprich, A. D. Daniels, Ö. Farkas, J. B. Foresman, J. V. Ortiz, J. Cioslowski, D. J. Fox, *Gaussian, Inc., Wallingford CT* (**2009**).